Journal of Engineering Science and Technology
Vol. 17, No. 3 (2022) 2049 - 2066
© School of Engineering, Taylor's University

EXPERIMENTAL ANALYSIS OF THERMAL PERFORMANCE OF A SOLAR AIR HEATER WITH A FLAT PLATE AND METALLIC FIBER

MUHAMMAD ASMAIL ELEIWI[1,*],
MOHAMMED FOWZI MOHAMMED[2], KAMIL TALIB KAMIL[2]

[1]Department of Mech. Engineering, College of Engineering, Tikrit University, Tikrit, Iraq
[2]Department of Mechanical Engineering, University of Technology, Baghdad, Iraq
*Corresponding Author: muham76@tu.edu.iq

Abstract

This research is aiming to study the overall performance (η_{al}) of a solar air heater integrated system (SAHIs) beneath the conditions of the Iraq weather through the use of a flat plate with metallic fiber (FPMF) as a fresh technique in heat absorption with inexpensive price. Numerous experiments were first carried out utilizing a double-pass flat plate and then compared with using a flat plate (FP) and metallic fiber (MF) solar air heater (SAH) as absorber surface (AS). Such experiments were conducted through March, and April of 2019 over a range of the air mass flow rate $\dot{m}_a$ (0.0071-0.0126 kg/s) and relying on the ecological conditions. The outcomes manifested that the η_{al} of SAH was (45.63%) and (88.5%) with a flat absorber plate (FAP) and (FPMF), respectively when using $\dot{m}_a$ =0.0126 kg/s. It was found that at $\dot{m}_a$ = 0.0126 kg/s, the maximum temperature of AS and the outlet air was 52.5°C and 34°C for the FAP, correspondingly and 41 °C and 39.5 °C for the FPMF, respectively. As well, the results manifested that, if utilizing the FPMF, the η_{al} of SAH was higher than that when using just FAP at the same $\dot{m}_a$. In addition, the temperature difference between the AS and the air of outlet when using FPMF was less compared with the utilization of FAP, and the discrepancy between the inlet air temperature (T_i) and the outlet air temperature (T_{out}) reduced if the $\dot{m}_a$ was raised. Furthermore, the current work evinced a higher η_{al} than those found via preceding works.

Keywords: Flat plate, Flat plate with metallic fiber, SAH.

1. Introduction

The solar air heaters (SAHs) were extensively used in different industrial applications and household. Techniques of artificial flow modification were provided in the field of flow to improve the thermal efficiency of SAH. Consequently, the laminar sublayer under the absorber plate (AP) will be disturbed and this leads to raise the turbulence level of air. Using different shaped turbulators helps improve the thermal performance of SAH since they raise the heat transfer rate (HTR) from the (AP) [1].

Acır et al. [2] studied the Energy and Exergy efficiencies of a SAH by experimental tests. The study was performed for a circular shaped turbulator with a variable hole number (HN) equals (2), (4) and (6) inserted in a plain tube and m_a.(0.0023, 0.0033, 0.0044 and 0.0055 kg/s). It was found that the improvement increase of the SAHs was enhanced by reducing the HN on the circular tabulators and raising the m_a. The optimum value of the energy and exergy efficiencies was found (58.3±0.63 % and 20.7±1%) at noon, respectively, for the HN equals (2) and $\dot{m}_a$ (0.0055 kg/s).

Lati et al. [3] performed three experimental tests for a passive SAH with a FAP and laminated with a local sand thin layer. The first test was for selecting the best sand was taken from three various locations in the Algerian desert and it was treated as porous, the 2nd experimental test was to study the influence of the thickness of sand layer on the collector daily efficiency, and the third test was to investigate the effect of the sand diameter. Results manifested that the maximum efficiency was (62.1%) and (41.71%) for (0.063 mm) and (0.25 mm) particle diameter, respectively, the collector efficiency increased with the increasing of the sand layer thickness, and the best collector efficiency was (41.14%) for (0.84 mm) thickness of the sand layer.

Chabane et al. [4] conducted an experimental investigation for a flat plate SAH in the hall of Mechanical Engineering Department in the Biskra University. Rectangular baffles were added perpendicular to the stream of air to decrease the thermal losses and increase the discrepancy of temperature of the outlet and inlet temperature. The experiment was categorized into various modes. Every mode possesses its own assignment and a certain no. of baffles. The outcomes evinced that the thermal efficiency with the median and the whole placement transversal baffles of a SAH was higher than the other mode, employing the similar number of baffles as well as airflow rate.

Kumar et al. [5] presented an experimental study to a fluid flow turbulent convection throughout an impingement round jet SAH rectangular passage with a circular inside obstacle with conical ring shapes. The solar air rectangular tests contained: the relative inside height of conical ring (HR/DH) from (0.073 to 0.128), the ratio of the inlet flow diameter to the ring inner print diameter (DIR/DBR) from (1.3) to (2.3), the ratio of diameter to the height of ring (DO/HR) from (1.67) to (2.67), the relative X-axis pitch (XS/DO) from (4.71) to (7.71), the relative *y*-axis pitch (YS/DO) from (2.92) to (5.14), the relative impingement round jet diameter (DIJ/DH), the relative X-axis distance of jet (Ximp/DH), the relative Y-axis distance of jet (Yimp/DH), and the Reynolds number (Re) from (5000-230000). It was found that the highest value of the thermal performance and hydrodynamic was at (HR/DH equals 0.11), (DIR/DBR equals 1.7), (DO/HR equals 2.33), (XS/DO

equals 5.28), (YS/DO equals 3.42), (DIJ/DH equals 0.055), (Ximp/DH equals 0.366), and (Yimp/DH equals 0.311).

Salih et al. [6] studied the influence of the integrated paraffin Wax-PCM as latent heat storage upon the double-pass SAH performance. An indoor projector simulator was utilized for testing a fresh regime through the process of charge/discharge. It was found that the increase in airflow decreased the wax melting temperature and delayed the melting time during the charging process. Also, the optimum period of discharging and the rise of air temperature of heater for different solar intensities of (825), (725), and (625) $W.m^{-2}$ were attained after (3 hr) with (17.95 - 3 ºC), (2 hr) with (14 - 3ºC), and (1.25 h) with (11 - 2.5 ºC), at the similar speed of airflow (0.6 kg/min), correspondingly.

Eleiwi and Shallal [7] presented an experimental investigation for evaluating the overall thermal performance of a V-corrugated absorber SAH combined with an air-water heat exchanger (HE) with and without using reflectors in Iraq-Samarra. The HE was employed for compensating the sun nonappearance prior to the sunrise and beyond the sunset. The maximum η_{al} was found to be (63.4%) and (59.9%) at the m_a (0.017 kg/s) with and without using reflectors, respectively, and the HE was contributed to reducing the fuel consumption to (65.04%) per month through the period of sun absence.

Yassen et al. [8] conducted an experimental work to investigate the effect of a triangular plate and MF as an absorber surface on the η_{al} of SAH. It was found that the η_{al} was (63.77%) and (74.2%) for the triangular plate and MF, respectively at m_a (0.0125 kg/s).

The aim of the present work is to study the SAH for domestic heating which it consists of a FP and a FPMF as absorber surface to enhance the η_{al} to the best level and this fresh technique in this study is an enhanced innovation. A work being performed under an operation and environment conditions of Baghdad city in Iraq.

2. Methodology

In the experimental part, the SAH system design, working principle, and measurement devices are described in detail. The components of the experimental rig of the system of the SAH include an AS as a FP and a FPMP, a glass cover and an insulated box.

2.1. SAH design of system

The SAH experimental test rig was installed in Baghdad city with 45º tilt angle from the horizontal opposing to south. The integrated SAH regime includes a galvanized steel plate box having (1.25 m) length (L_p), (0.25 m) width (W_p), (15 cm) height (W_s), and (2 mm) thickness. A single glass layer was used as a transparent cover of the collector with (7 mm) thickness. To decrease the losses of heat by conduction, a glass wool insulation was used as thermal insulator possessing a 2 cm thickness for sides and base, as shown in Fig. 1(a) FP and a FPMF are installed inside the SAH as an absorber surface, the FP and the MF are made from steel (A36), with an inexpensive price.

The MF is strip wires that have a shape of a rectangular cross section with dimensions (0.2 mm × 3mm).The FP has (1.24 m) length (L_t), and (9 cm) width

(W_t). Both FP and MF being dark black painted with an available paint in the local market for the heat absorption. Silicon substance was used to reduce heat loss from glass sides, and to prevent water rain, and water dust from the entering into the solar collector. Further details on the system design are comprised in Table 1.

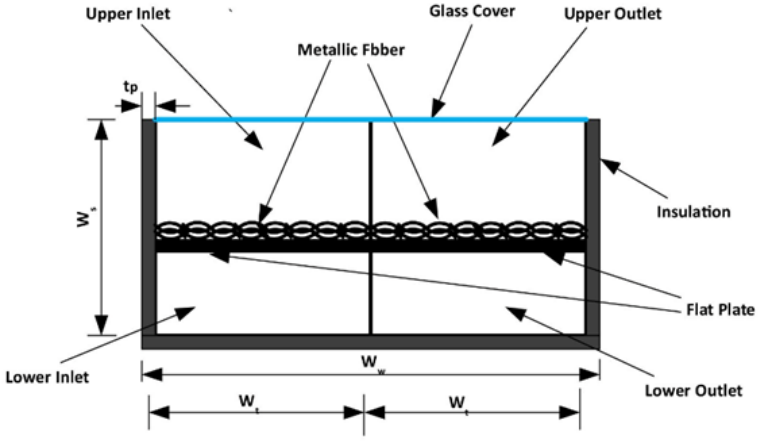

(a). FPMF

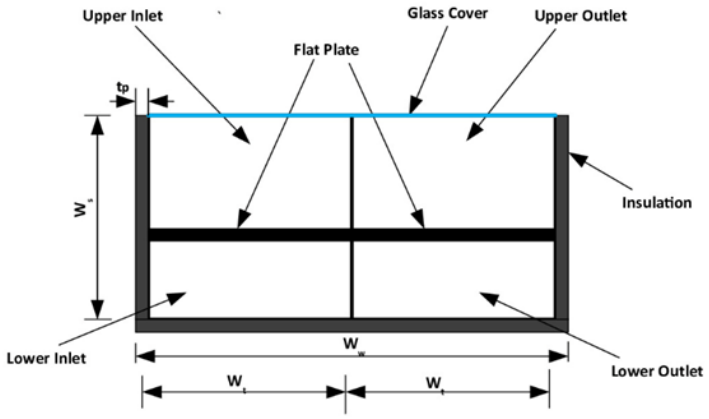

(b). FP

Fig. 1. The solar air heater schematic diagram showing the dimensions of design.

Table 1. Design parameters of SAHIs.

Collector	**SAH**
L_p : Length	1.25 m
W_p: Width	0.25 m
W_s: Height	15 cm
α : Angle of inclination	45°
Absorber plate	**FP & MF**
FP	
Material	Galvanized steel gage (2 mm)

L_t : Length	1.24 m
W_t : Outlet and inlet width	9 cm
t_p : Thickness	3.5 cm
MF	
Material	Mild Steel
Shape	Rectangular strip wires
Dimensions	0.2 mm × 3mm
Mass	0.52 kg
The colour of paint	Black
Type of absorber	Matte
Absorptivity	0.85
Transparent cover	Glass
The layer number	Single
Thickness	7 mm
Insulation	Glass wool
Thickness	2 cm

2.2. Experimental installation and used instrument

To measure the temperature at different locations for the SAH in the system, UT325 a digital thermometer possessing (±0.2%) accuracy was used. Type K thermocouple (Chromel-Alumel) was utilized, this can be used for measuring the temperature in the range (-200-1372 ^{o}C).

The measurement of the temperature distribution of the AP was done by using four thermocouples, three thermocouples were located on the lower exit, and three thermocouples were placed on the upper exit of SAH to measure the average temperature on the lower and upper exit, respectively.

The inlet air temperature to collector was measured by using one thermocouple. The incident solar power radiation on the collector was recorded by Digital Solar Meter (Type TES) Solar Power Meter (TES-13334) possessing (±5%) accuracy. Such instrument measures the whole solar radiation (beam and diffuse) per unit area of collector surface.

The solar power meter being oriented toward the south at a tilt angle (45° south) of collector. Such angle was adopted for the whole examination cases. (WS-1000-WiFi), as a type of digital ambient weather with (±5%) accuracy, was employed for quantifying the relative humidity of weather, and (405-V1) as a Digital Thermo-Anemometer with (±5%) accuracy was utilized for quantifying the speed of air through the fan. Figure 2 reveals the setup of experiment in this investigation.

3. Experimental Method

The outdoor experimental test rig of SAH was installed in Baghdad city with 45° tilt angle from the horizontal opposing to south to investigate the SAH system performance. The measurements of V, T_{mb}, $\emptyset$, T_{out} and the T_{sb} were registered each half hour, also all tests were carried out from (9:00 am) to (4:00 pm). The experimental test rig of the designed as well as fabricated system of SAH is depicted in Fig. 3.

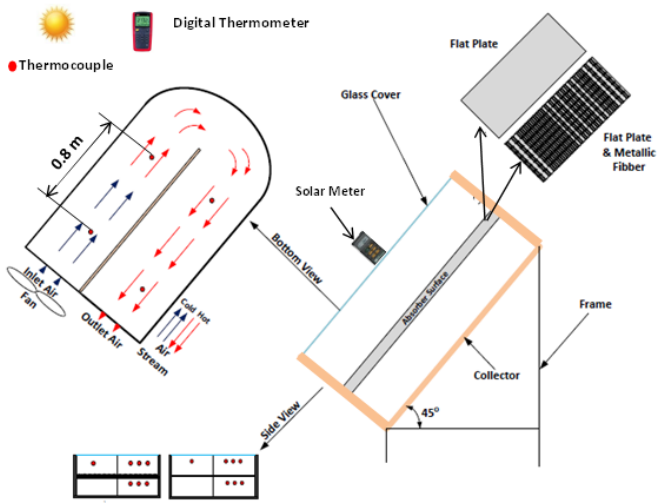

Fig. 2. Experimental setup SAHIs.

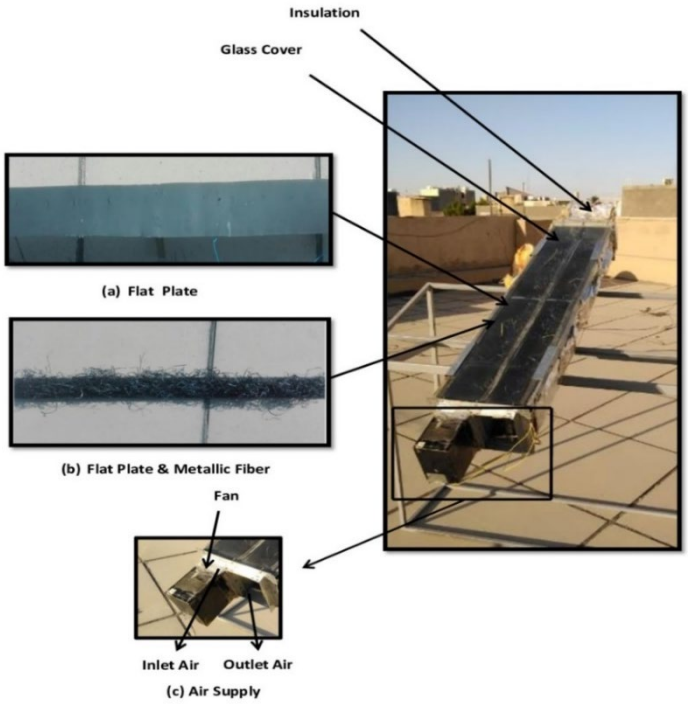

Fig. 3. Solar air heater experimental test rig.

4. Theoretical Background

The heat input to the SAH [8]

$$Q_{in} = \int_0^t IA\,dt \tag{1}$$

where t is the global solar radiation time through a day and I is the average solar radiation per day, W.m^{-2}

The output heat from the SAH [9]

$$Q_{out} = \dot{m}_a C_p \int_0^t (T_{out} - T_i)\, dt \quad (2)$$

where $\dot{m}_a$ is the drain of the $\dot{m}_a$ from the SAH and Cp is the heat capacity of air, kJ/kg.K

The thermal efficiency per day [10]

$$\eta_{al} = \frac{Q_{out}}{Q_{in}} \quad (3)$$

When Eqs. (1) and (2) are substituted into Eq. (3), the SAH mean daily efficiency [7] can be computed as

$$\eta_{al} = \frac{\dot{m}_a C_p \int_0^t (T_{out} - T_i) dt}{\int_0^t I A d_t} \quad (4)$$

5. Experimental Uncertainty Analysis

All the quantities that are measured to estimate the independent parameters (such as fan speed, solar radiation, relative humidity and temperature). Here, such separate uncertainties are introduced. The analysis was performed upon the foundation of the proposal prepared via the bias of error (B), precision limit (P), utilizing of the Collect-Root-Sum Squares method (RSS). In this study, the errors can be clearly categorized into three sets of the error of calibration, decrease of data, and gathering of data.

The bias error (B) can be obtained by the following equations [11].

$$B = \pm[(\tfrac{1}{2}\text{Resolution})^2 + (\text{Accuracy})^2]^2 \quad (5)$$

The average value of scale or the measuring average is

$$\bar{X} = \frac{1}{n}\sum_{i=1}^{n} Xi \quad (6)$$

The sample distribution standard deviation (σ) is

$$\sigma x = [\frac{1}{n-1}\sum_{i=1}^{n}(Xi - \bar{X})^2\ ]^{\frac{1}{2}} \quad (7)$$

The sample's average standard deviation ($\sigma\bar{X}$) was inferred utilizing this relationship:

$$\sigma\bar{X} = \frac{\sigma x}{\sqrt{n}} \quad (8)$$

By using the t-distribution at a confidence level of 95% with (N-1) degrees of freedom, all exactness limits of error are stated as following:

$$Px = t(N-1), 95\% \times \sigma\bar{X} \quad (9)$$

For getting an uncertainty (Ux) confidence of 95%, integrating the elemental errors has to be conducted.

$$Ux = \pm[B^2 + Px^2]^{\frac{1}{2}} \quad (10)$$

The comparative uncertainty (in percentage) is computed as:

$$\frac{Ux}{X}\% = \pm\left(\frac{Ux}{x}\right) \times 100 \quad (11)$$

The computed uncertainty for the parameters mentioned in this section has been given in Table 2. (*X*) being utilized as an independent parameter. Consequently, uncertainty of (±8.8%) was for solar radiation (*I*), of (±13.63%) for speed of fan, and of (±14.72%) for relative humidity. Additionally, the ambient temperature predicted uncertainty being (±4.27%), also the AS temperature and the T_{out} being (±4.82%) and (±5.06%), correspondingly.

Table 2. Uncertainty of the measured parameters.

	B	$\overline{x}$	σ_x(dev.)	$\sigma_{\overline{x}}$ (dev.)	P_x	U_x	$\frac{U_x}{x}$%
I (W.m^{-2})	±0.07	920.27	50.93	25.46	81.03	81.035	±8.8
Ø	±0.05	0.56	0.035	0.02	0.066	0.082	±14.72
V(m/s)	±0.05	0.663	0.047	0.023	0.075	0.09	±13.63
T_o (°C)	±0.05	34.62	1.1	0.55	1.76	1.766	±5.06
T_s (°C)	±0.05	50.56	1.53	0.766	2.43	2.43	±4.82
T_i (°C)	±0.053	26	0.81	0.4	1..30	1.076	±5

6. Results and Discussion

The performance experimental test of the entire system on the environmental conditions (sunny day) of Baghdad city (in Iraq) is introduced in the present section. This experimental test was conducted through March and April of 2019, using a FP and a FPMF as an AS in this test from (9:00 am) until (4:00 pm).

6.1. SAH with a FP

To study the overall performance of the SAH system, such system was examined utilizing a FP as an AS from (9-03-2019) to (21-03-2019) for reducing the varying influence of the solar intensity and the ambient conditions. Results of such test are revealed in Figs. 4 to7.

Variation of the relative humidity (Ø) and the solar energy with local time, and the maximum I of 980 W.m^{-2} on 9 of March, (970) W.m^{-2} on 15 of March, (958) W.m^{-2} on 16 of March, and 970 W.m^{-2} on 17 March are shown in Figs. 4(a) to 7(a), correspondingly. One can see that the *I* begin to increase from the first hr (9:00 am) of the test and attains the ultimate value at (12:00 pm), as displayed in the Fig. 7(a) at (12:30 pm), as illustrated in the Figs. 5(a) and 6(a), and at (1:00 pm), and as evinced in Fig. 4(a), after that, it starts decreasing slowly till reaching the final test hour at (4:00 pm). Also, *Ø* first begins with higher values, and after that, it slowly reduces with the hours of daylight.

The ambient temperature variation, the mean T_{out}, and the average AS temperature with local time at $\dot{m}_a$ (0.0025, 0.0071, 0.0099 and 0.0126 kg/s) of air, are elucidated in the Figs. 4(b), 5(b), 6(b) and 7(b), respectively. It is observed that the average temperature of AS and the average T_{out} are 53.7 °C and 41 °C, respectively in Fig. 4(b), 49.75 °C and 37.5 °C in Fig. 5(b), 52.5 °C and 36 °C in Fig. 6(b) and 52.5 °C and 34 °C in Fig. 7(b).

These temperatures first increased by increasing *I*, after that they decreased in a gradual with *I* decrease. The reason for that is a decrease in the amount of absorbed energy which is slightly lower than the heat losses, and that results in a decrease in the useful energy moving to the SAH air.

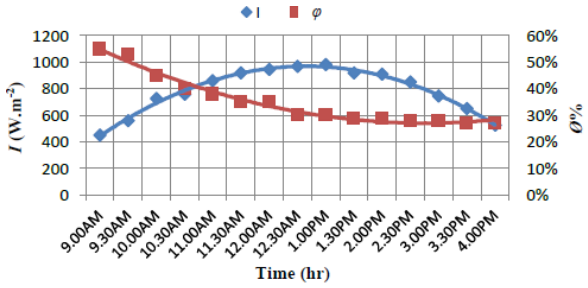

(a)

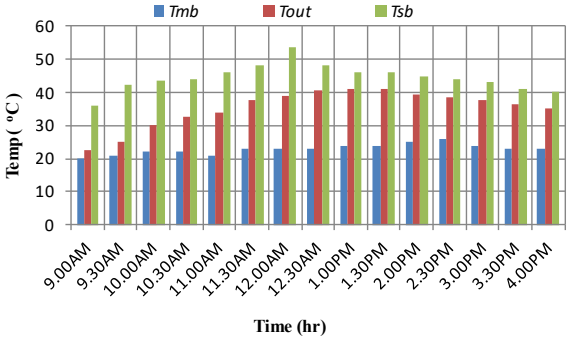

(b)

Fig. 4. (a) Variation of the *I* and *Ø* with local time on 9/03/2019, (b) The temperature change with local time at ($\dot{m}_a$ = 0.0025 kg/s), using FP.

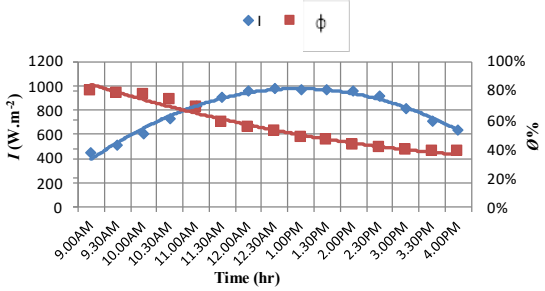

(a)

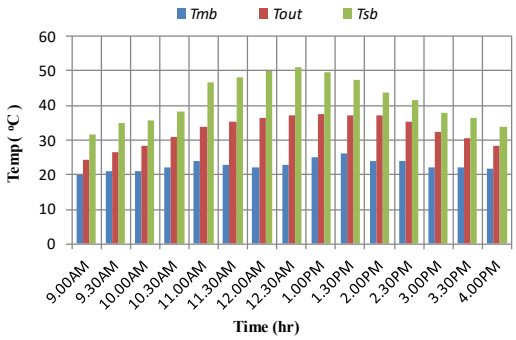

(b)

Fig. 5. (a) Variation of the *I* and *Ø* with local time on 15/03/2019 , (b) The temperature change with local time at ($\dot{m}_a$ = 0.0071 kg/s), using FP.

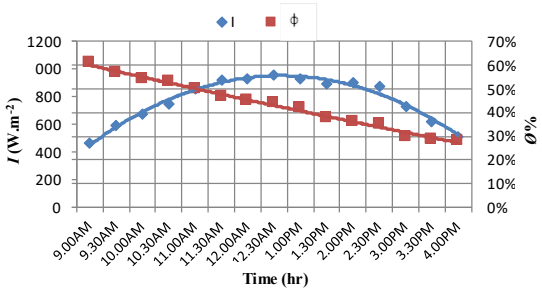

(a)

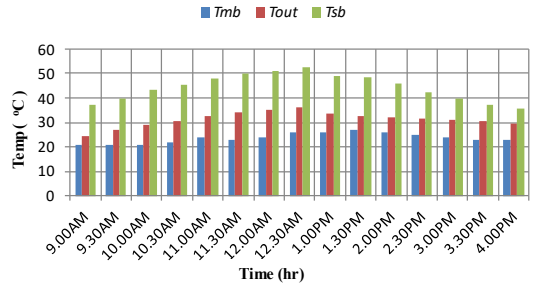

(b)

Fig. 6. (a) Variation of the *I* and *Ø* with local time on 16/03/2019, (b) The temperature change with local time at ($\dot{m}_a$ = 0.0099 kg/s), using FP.

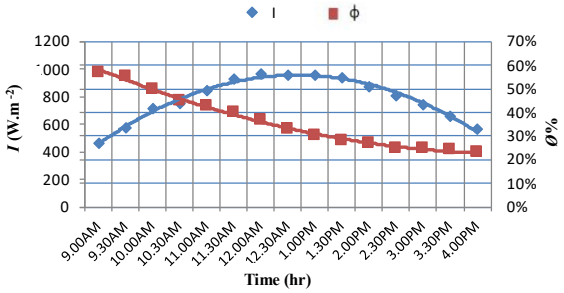

(a)

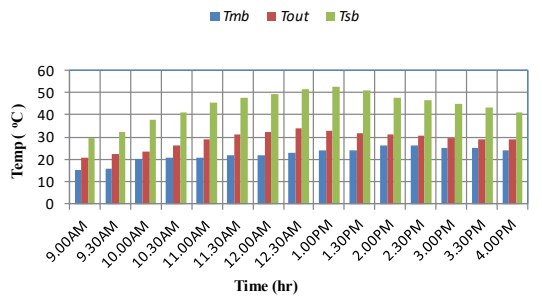

(b)

Fig.7. (a) Variation of the *I* and *Ø* with local time on 21/03/2019, (b) The temperature change with local time at ($\dot{m}_a$ = 0.012 kg/s), using FP.

6.2. Solar air heater with a FPMF

The overall performance of the SAH system was introduced during April (2019); such system was tested utilizing a MF at different $\dot{m}_a$. The outcomes of the overall performance of the SAH system utilizing a FP and MF as an AS are manifested in Fig. 8.The *I* variation and *Ø* with local time are manifested in Figs. 8(a), 9(a), 10(a) and 11(a).

The maximum I was 992 W.m^{-2} on 13 of April. One can notice that the *I* first begins increasing from the test first hr (9:00 am) and attains the ultimate value at (12:00 pm as displayed in Figs. 8(a) and 11(a), at (12:30 pm) as demonstrated in Fig. 8(a), and at (1:00 pm) as revealed in Fig. 9(a) and after that, it starts to drop slowly till the test final hr at (4:00 pm). *Ø* first begins with higher values and after that, it slowly reduces with the hours of daylight.

The variation of ambient temperature, the outlet mean temperature and the average AS temperature with the local time at $\dot{m}_a$ (0.004, 0.007, 0.0098 and 0.0126 kg/s) of air, correspondingly are elucidated in Figs. 8(b), 9(b), 10(b) and 11(b). It was observed that the maximum average AS temperature and the mean T_{out} are (49.5 °C and 46 °C), respectively in Fig. 8(b), (48 °C and 42.5 °C) in Fig. 9(b), (42.75 °C and 39.5 °C) in Fig. 10(b), and (41 °C and 39.5 °C) in Fig. 11(b). Those temperatures first elevated with the I increment, and after, they decreased in a gradual way with the *I* decrease, for same cause in the Figs. 4(b), 5(b), 6(b) and 7(b). The overhead outcomes stated that the temperature of AS and the T_{out} are greater if using FPMF in comparison with FAP. This is due to that the FPMF increases the HTR via stirring the flow and via providing a big surface of contact, which results in an increase in the useful energy moved to the SAH.

One can note in Figs. 4(b) to 11(b) that the temperature discrepancy between the outlet and inlet air reduces with the $\dot{m}_a$. increase, since if the air flow rate is higher, then air will possess less time for transferring the heat and that results in a lesser change in temperature. Also, it can be observed that the temperature discrepancy between AS and outlet air at using a FP was bigger compared with using a FPMF as an AS because MF provides an additional surface area for the heat transfer.

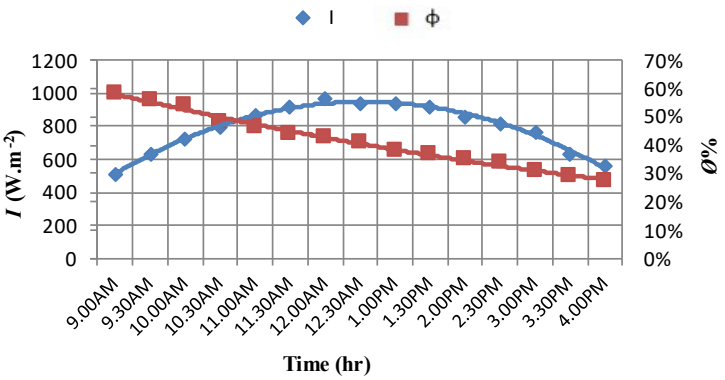

(a)

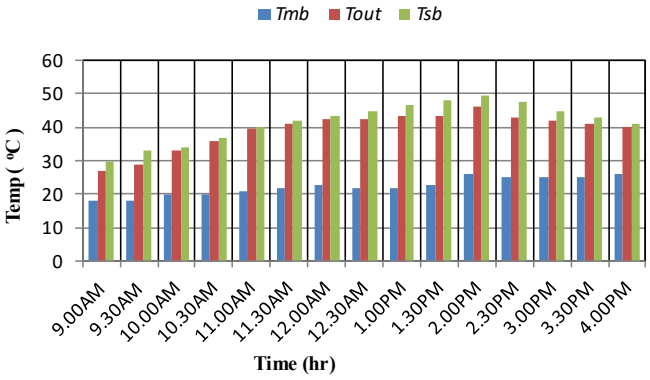

(b)

Fig. 8. (a) Variation *I* and *Ø* with local time on 12/4/2019 , (b) The temperature change with local time at ($\dot{m}_a$ = 0.004 kg/s) , utilizing FPMF.

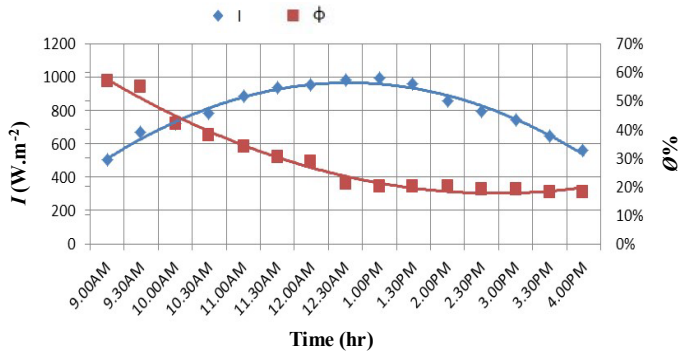

(a)

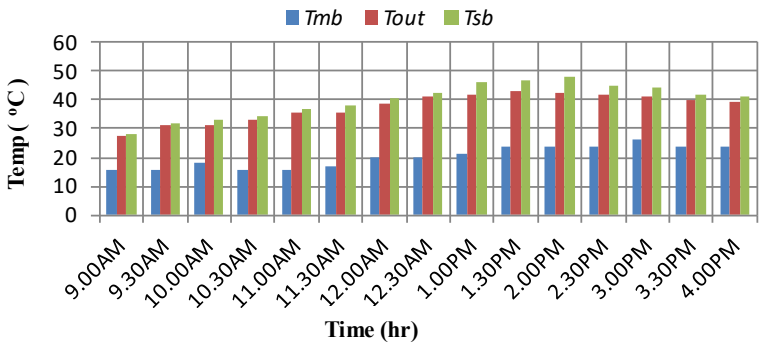

(b)

Fig. 9. (a) Variation of the *I* and *Ø* with local time on 13/4/2019 , (b) The temperature change with local time at ($\dot{m}_a$ = 0.007 kg/s) , utilizing FPMF.

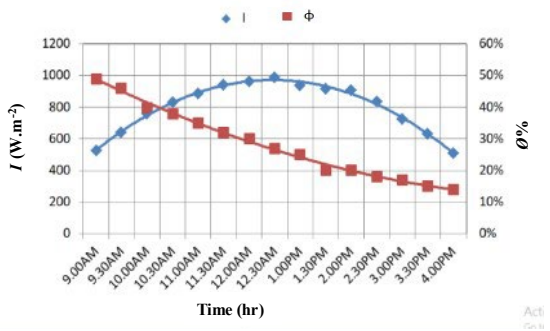

(a)

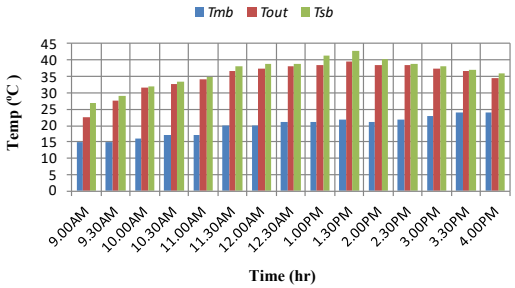

(b)

Fig. 10. (a) Variation of *I* and *Ø* with local time on 17/4/2019 , (b) The temperature change with the local time at ($\dot{m}_a$ =0.0098 kg/s), using FMPF.

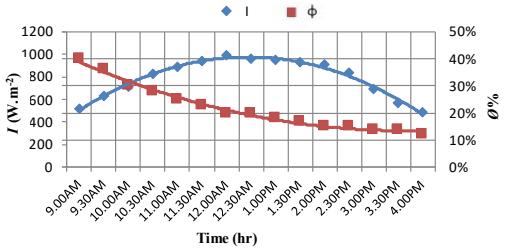

(a)

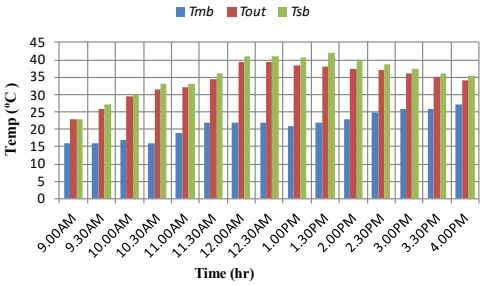

(b)

Fig. 11. (a) Variation of the *I* and *Ø* with local time on 21/4/2019, (b) The temperature change with the local time at ($\dot{m}_a$ = 0.0126 kg/s) on 21/4/2019, utilizing FPMF.

6.3. The overall thermal efficiency of the soar air heat

Figure 12 depicts the variation of energy balance and the η_{al} for different air mass flow rates. The input energy being the quantity of energy got from the I, and the energy amount transported by air, which is the discharged air from the system, being the output energy, via utilizing FPMF ,the output energy being more if compared with utilizing a FP since the FPMF increases the heat transfer compared to just FP.

The relationship between the mean η_{al} of SAH, if utilizing a FP in addition to a FPMF as an absorber surface, and the $\dot{m}_a$ is illustrated in Fig. 13. It can be noted that the η_{al} increases significantly with increasing of the $\dot{m}_a$ due to the decrease in the temperature of AS and that causes a drop in the thermal losses.

The maximum η_{al} being (45.66%) and (88.5%) at the $\dot{m}_a$ (0.0125 kg/s) if utilizing FP and FPMF as an AS, respectively. When using FPMF, η_{al} of SAH is bigger compared to the FP, since the FPMF raises the HTR in comparison with the amount of HTR used with the FP as an AS. And after that, it results in less change between the T_{as} and the T_{out}, causing a high energy.

Figure 14 reveals the relation between η_{al} and $\dot{m}_a$ for FP, MF, FPMF, and triangular plate. The outcomes manifested that the ultimate η_{al} took place at FPMF because the MF provides additional surface area for heating in addition to FP surface area.

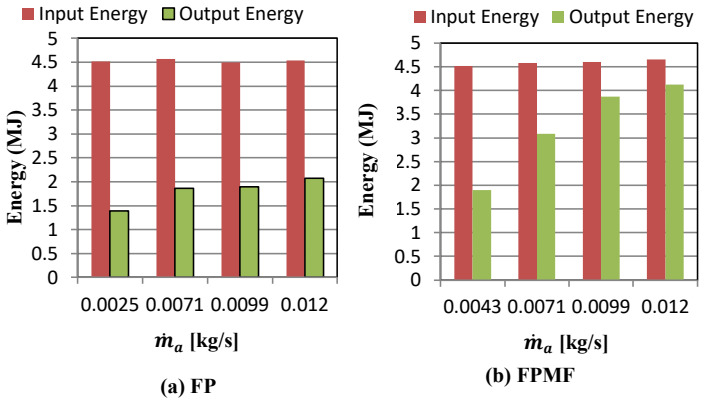

Fig. 12. Energy variation with the $\dot{m}_a$during the period (9:00 am to 4:00 pm).

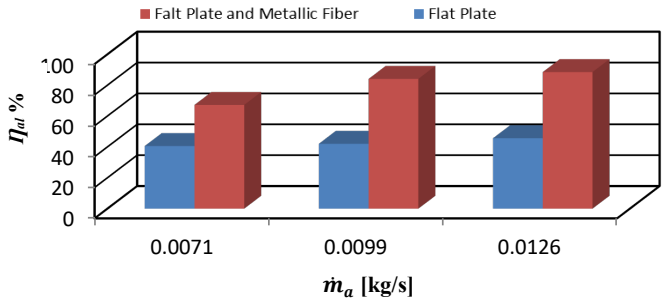

Fig. 13. The overall thermal efficiency of the soar air heat, η_{al} vs. mass flow rates, $\dot{m}_a$.

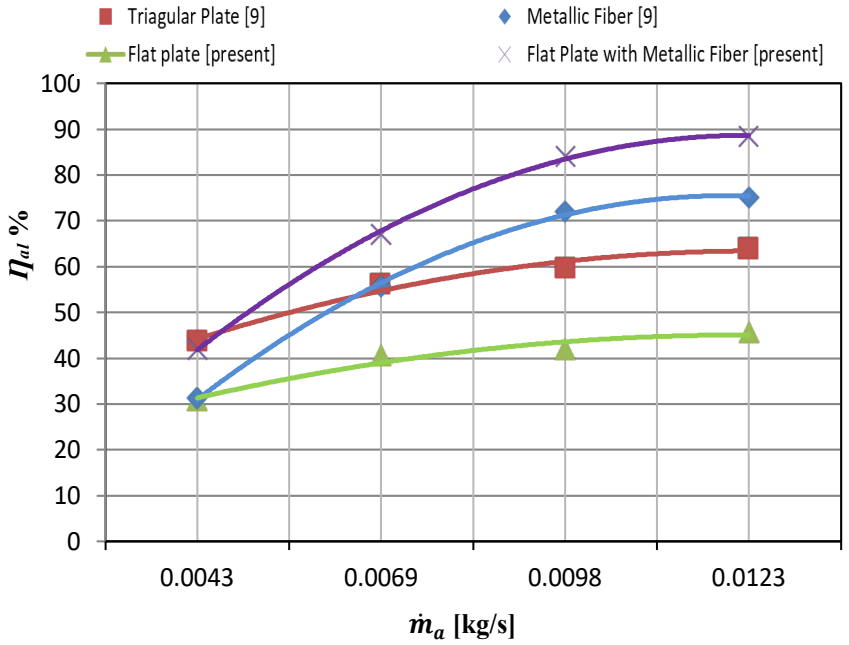

Fig. 14. The overall thermal efficiency of the soar air heat, η_{al} vs. mass flow rates, $\dot{m}_a$.

6.4. Comparison between the present investigation and the previous studies

Table 3 displays a comparison between the present investigation and the previous studies in computing η_{al} of a double-pass SAH with FP and FPMF. Concerning the experimental study,

- η_{al} in a previous work Mahmood [12] was 86% at $\dot{m}_a$= 0.018 kg/s, whereas in the current work, it was 88.5% and 45.63% with a FP and a FPMF, respectively at $\dot{m}_a$ = 0.0125 kg/s, although m_a of the present work is less than the previous study, but weather conditions of the present work are better than those in the previous study. Also, the utilizing of a FPMF resulted an increase in the temperature of airflow although the AS in the earlier work being done from two steel galvanized cover, perforated AP and six layers of wire mesh having good heat transfer. In addition, utilization of a double-glass cover reduced the heat losses more than a single-glass cover.
- Comparing to the preceding work of Eleiwi and Shallal [7] who obtained that η_{al} being 63.49% and 59.9% with and without utilizing reflectors, correspondingly at $\dot{m}_a$ = 0.017 kg/s, η_{al} in this research was obtained higher if utilizing a FPMF despite the preceding work employed reflectors and a high $\dot{m}_a$.
- When utilizing the $\dot{m}_a$= 0.0125 kg/s, η_{al} with the previous study Mohammed et al. [13] was low employing a triangular plate and just MF compared to the present study if employing a FPMF.

Table 3. Comparison between experimental results of the present study and previous studies.

Operating time	$\bar{I}$ (W.m^{-2})	$\overline{T_a}$ (°C)	A_a (m^2)	*Ng*	Material type of the absorber surface	$\dot{m}_a$ (kg/s)	η_{al} (%)	Ref.
8:00 am to 4:00 pm	598.8	17.8	1.5	Un-glazed	Perforated absorber plate and six wire mesh layers	0.018	86 without reflectors	[12]
9:00 am to 4:00 pm	689.25	13.93	0.902	1	Galvanized steel-corrugated -plate	0.017	59.59 without reflectors	[7]
	964	14.89	0.902	1	Galvanized steel corrugated -plate	0.017	63.49 with reflectors	
9:00 am to 4:00 pm	801.466	21.86	0.22	1	Galvanized steel-triangular plate	0.012	63.77 without reflectors	[13]
	779.86	20.66	0.22	1	Galvanized steel-MF	0.012	74.2 without reflectors	
9:00 am to 4:00 pm	782.93	22.26	0.22	1	Galvanized steel-FP	0.012	45.63 without reflectors	Present
	789.06	23.73	0.22	1	Galvanized steel-FPMF	0.012	88.5 without reflectors	

7. Conclusions

In the present study, a SAH with a FP and a FPMF as an AS has been studied experimentally at various $\dot{m}_a$. η_{al} of the solar air was calculated, and the resulted outcomes were compared with preceding investigations. Depending on the obtained result of this study, throughout this, the following conclusions can be drawn:

- The η_{al} of the SAH with a FPMF was higher than that with a FP as AS at the same $\dot{m}_a$.
- The FPMF gives the SAH a large amount of the HTR compared to that of the FP, and this in turns results an increase in T_{sb} and T_{out}.
- The temperature difference between the AS and the outlet air, if using a FPMF, is less compared to that with the FP utilization.
- The current investigation elucidated a higher η_{al} than those determined via the preceding investigations.

Acknowledgements

The authors are grateful to the Mechanical Engineering Department at the College of Engineering in Tikrit University for offering the laboratory facilities throughout performing the present research.

Nomenclatures

A	Area of Aperture, m^2
C_p	The specific heat of air, J/(kg K)

I	The solar radiation, W.m^{-2}
$\bar{I}$	The daily average solar radiation, W.m^{-2}
$\dot{m}_a$	Air mass flow rate, kg/s
Ng	The number of glasses
Q_{in}	The Inlet heat to SAH, J
Q_{out}	The outlet heat from SAH, J
Ti	The Inlet air temperature to SAH, ℃
T_{mb}	Ambient temperature, ℃
T_{out}	The mean outlet air temperature from SAH, ℃
T_{sb}	The mean surface temperature of the absorber plate, ℃
V	Fan speed, m/s

Greek Symbols

η_{al}	The overall thermal efficiency.
$\emptyset$	The relative humidity

Abbreviations

AP	Absorber plate
AS	Absorber Surface
FP	Flat Plate
FPMT	Flat Plate with Metallic Fiber
HS	Heat Storage
HSC	Heat Storage Capacity
HTR	Heat Transfer Rate
MF	Metallic Fiber
PCM	Phase Change Material
SACs	Solar Air Collectors
SAH	Solar -Air Heater
SAHIS	Solar -Air Heater Integrated System
SAHs	Solar -Air Heaters

Reference

1. Arunkumar, H.S.; Karanth, K.V.; and Kumar, S. (2020). Review on the design modifications of a solar air heater for improvement in the thermal performance. *Sustainable Energy Technologies and Assessments*, 39, 100685.
2. Acır, A.; Emin, M.; Canli, M.E.; Ata, I.; and Tanürün, H.E. (2019). Effects of a circular-shaped turbulator having varying hole numbers on energy and exergy efficiencies of a solar air heater. *International Journal of Ambient Energy*, 40(7),739-748 .
3. Lati, M.; Boughali, S.; Bechki, D.; Bouguettaia, H.; Mennouche, D.; Gana, N.; and Ghettas, S. (2019). Experimental investigation on effect of an absorber plate covered by a layer of sand on the efficiency of passive solar air collector. *International Journal of Green Energy*,16(6), 413-422 .
4. Chabane, F.; Grira, F.; Moummi, N.; and Brima, A. (2019). Experimental study of a solar air heater by adding an arrangement of transverse rectangular baffles perpendicular to the air stream. *International Journal of Green Energy*,16(14), 1264-1277 .

5. Kumar, N.; Kumar, A.; Maithani, R.; Thakur, R.; Kumar, R.; and Thakur, A. (2019). Effect of circular inside conical ring obstacles on heat transfer and friction characteristics of round jets impingement solar air rectangular passage. *International Journal of Green Energy*, 16(14), 1091-1104 .
6. Salih, S.M.; Jalil, J.M.; and Najim, S.E. (2019). Experimental and numerical analysis of double-pass solar air heater utilizing multiple capsules PCM. *Renewable Energy*, 143, 1053-1066 .
7. Eleiwi, M.A.; and Shallal, H.S. (2022). Thermal performance of solar air heater integrated with air-water heat exchanger assigned for ambient conditions in Iraq. *International Journal of Ambient Energy*, 43(1), 2153-2164.
8. Yassen, T.A.; Mokhlif, N.D.; and Eleiwi, M.A. (2019). Performance investigation of an integrated solar water heater with corrugated absorber surface for domestic use. *Renewable Energy*, 138, 852-860.
9. Talib, S.M.; Rashid, F.L.; and Eleiwi, M.A. (2021). The effect of air injection in a shell and tube heat exchanger. *Journal of Mechanical Engineering Research and Developments*, 44(5), 305-317.
10. Mokhlif, N.D.; Eleiwi, M.A. and Yassen, T.A. (2021). Experimental investigation of a double glazing integrated solar water heater with corrugated absorber surface. *Materials Today: Proceedings*, 42(Part 5), 2742-2748.
11. Abed, F.M.; Eleiwi, M.A.; Hasanuzzaman, M.I.; and Mohammed, K.I. (2020). Design, development and effects of operational conditions on the performance of concentrated solar collector based desalination system operating in Iraq, *Sustainable Energy Technologies and Assessments*, 42, 1-13.
12. Mahmood, A.J. (2020). Thermal evaluation of a double-pass unglazed solar air heater with perforated plate and wire mesh layers. *Sustainability*, 12(9), 3619.
13. Mohammed, M.F.; Eleiwi, M.A.; and Kamil, K.T. (2020). Experimental investigation of thermal performance of improvement a solar air heater with metallic fiber. *Energy Sources*, *Part A: Recovery*, *Utilization*, *and Environmental Effects*, 43(18), 2319-2338.